Supporting Information

A multifunctional polyimide nanofiber separator with a self-closing polyamide-polyvinyl alcohol top layer of Turing structure for high-performance lithium-sulfur batteries

Xiang Luo,[a,b,1] Xianbo Lu,[c,1] Ya Chen,[e,1] Xiaodong Chen,[a,b,d,*] Hele Guo,[a] Chunyu Song,[a] Nannan Wang,[a,*] Dawei Su,[b] Guoxiu Wang,[b] and Lifeng Cui[a,*]

[a] *School of Materials Science and Engineering, Dongguan University of Technology, Dongguan 523808, Guangdong, China*

[b] *Center for Clean Energy Technology, School of Mathematical and Physical Science, Faculty of Science, University of Technology Sydney, NSW 2007, Australia*

[c] *R&D Center, Shanghai Kingfa Sci. & Tech. Co., Ltd., Shanghai 201714, China*

[d] *Department of Applied Chemistry, School of Science, Xi'an Jiaotong University, Xi'an 710049, Shaanxi, China*

[e] *School of Physical Science and Technology, ShanghaiTech University, Shanghai 201210, China*

[1]These authors contributed equally to this work.

*Corresponding authors.

E-mail addresses: chenxd@dgut.edu.cn (X. Chen); wangnn@dgut.edu.cn (N. Wang); lcui@dgut.edu.cn (L. Cui).

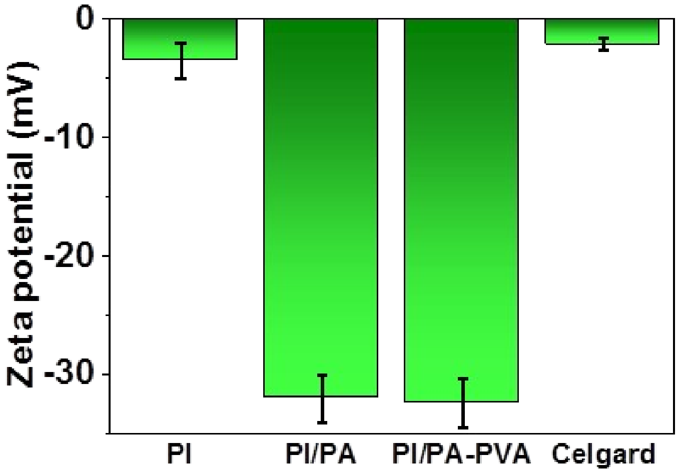

Figure S1. Surface zeta potentials of different separators.

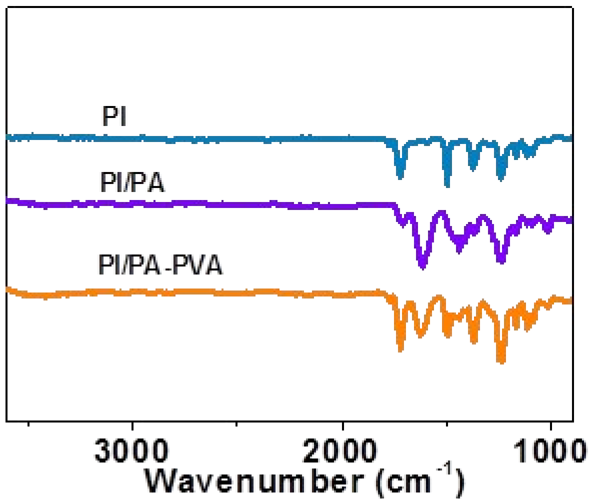

Figure S2. FTIR spectra of different separators.

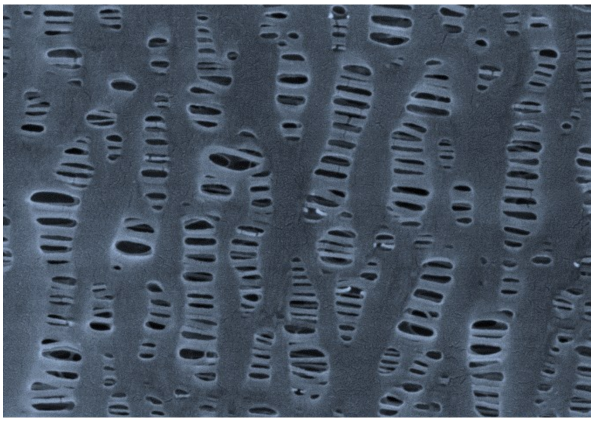

Figure S3. SEM image of the Celgard separator.

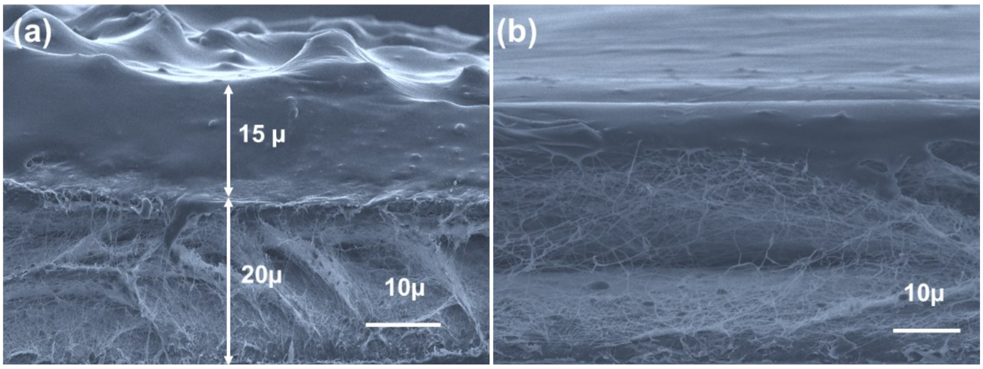

Figure S4. SEM images of cross-section of PI/PA-PVA separator: (a) fresh prepared, (b) after heating at 230 ^{o}C.

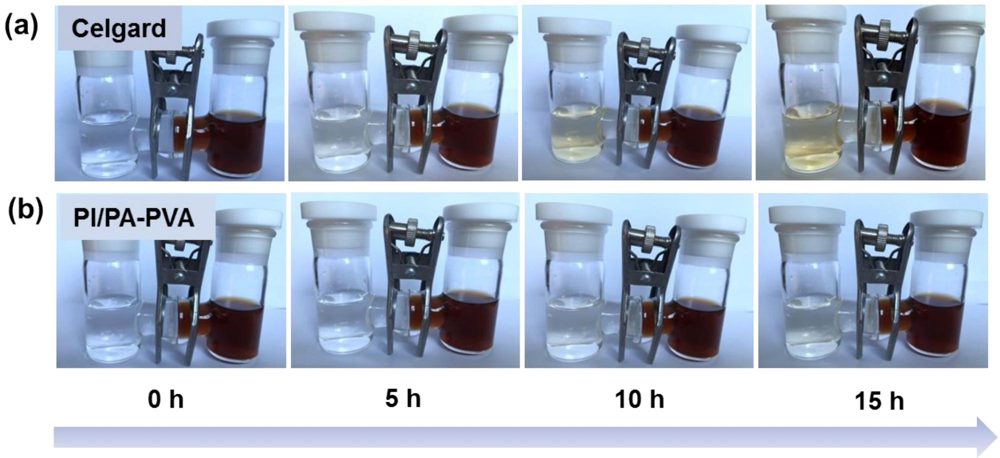

Figure S5. Photographs showing the polysulfide diffusion across the Celgard (a) and PI/PA-PVA (b) separators for different time, respectively.

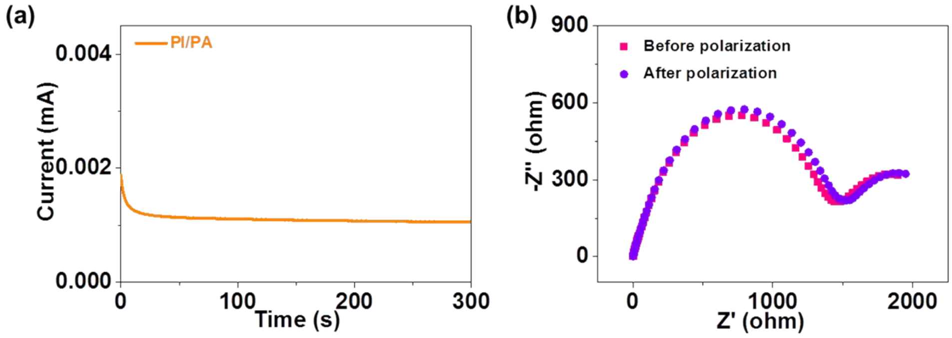

Figure S6. (a) Chronoamperometry profile of the PI/PA separator and (b) the corresponding impedances under the initial and steady-state current conditions.

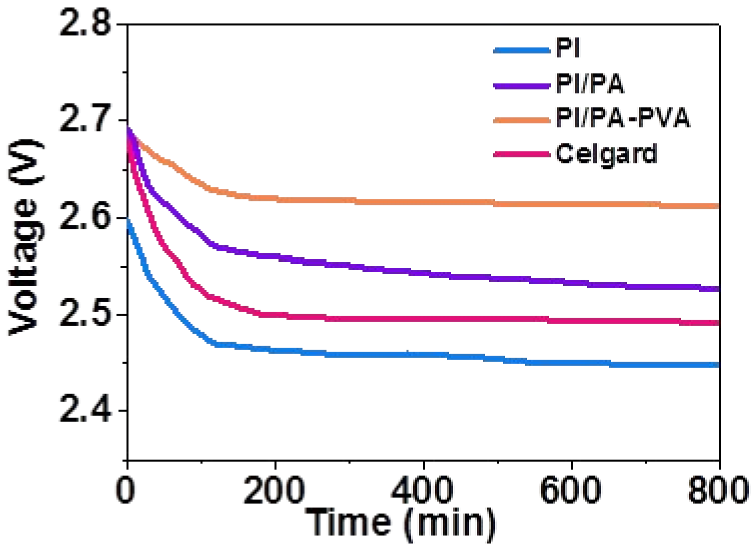

Figure S7. Open circuit voltage profiles showing the self-discharge behavior of Li-S batteries with PI, PI/PA-PVA and Celgard separators.

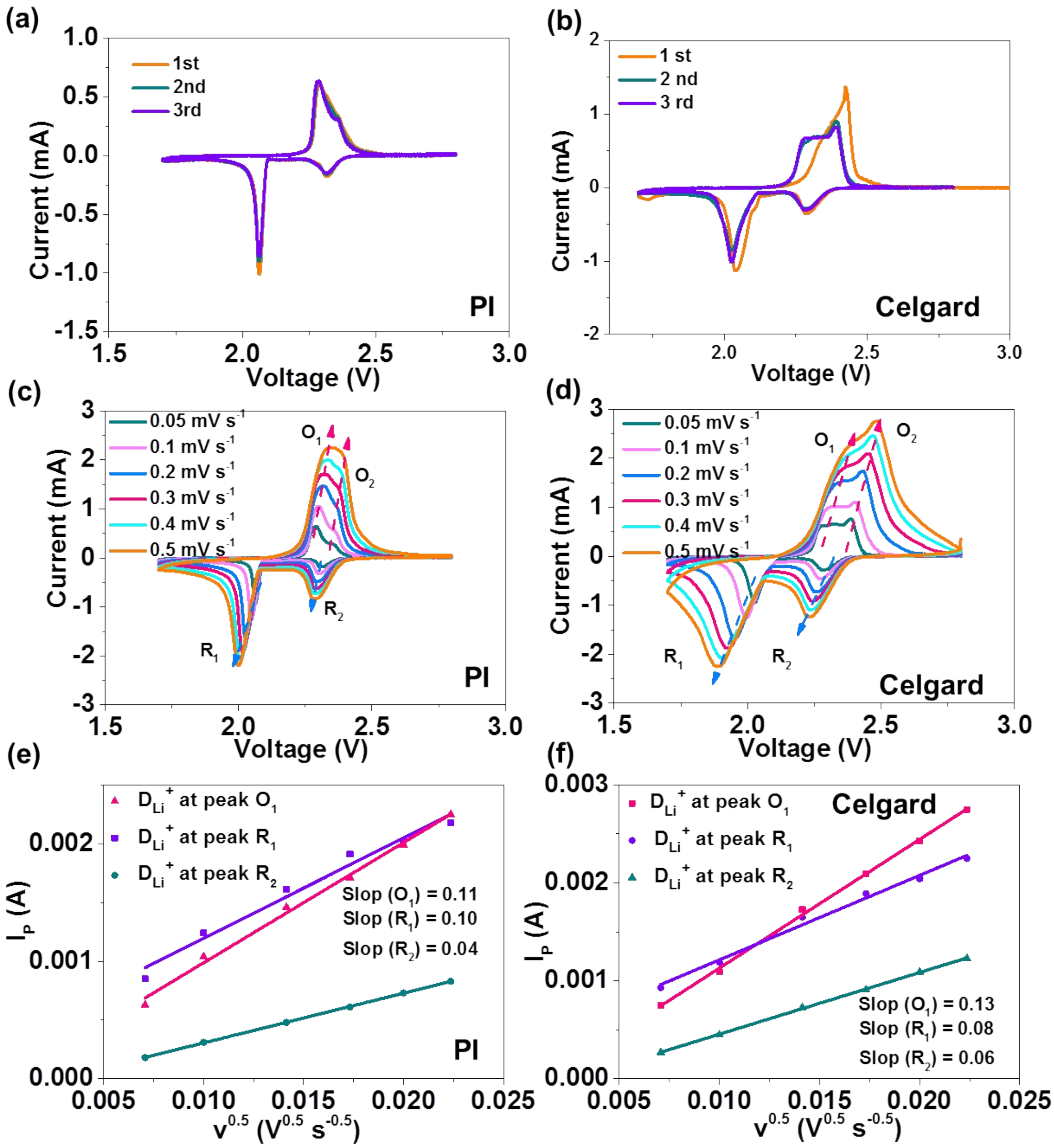

Figure S8. (a-b) CV curves of Li-S batteries with PI and Celgard separators at a scanning rate of 0.1 mV s^{-1}, (b-d) CV curves of Li-S batteries with PI and Celgard separators under different scanning rates and (e-f) the corresponding linear fits of the peak currents.

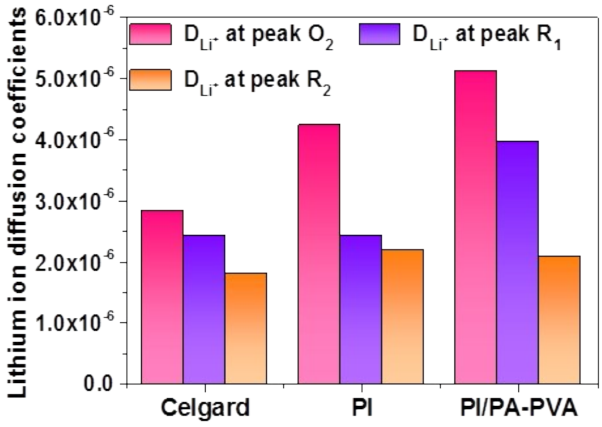

Figure S9. Lithium ion diffusion coefficients for different separators

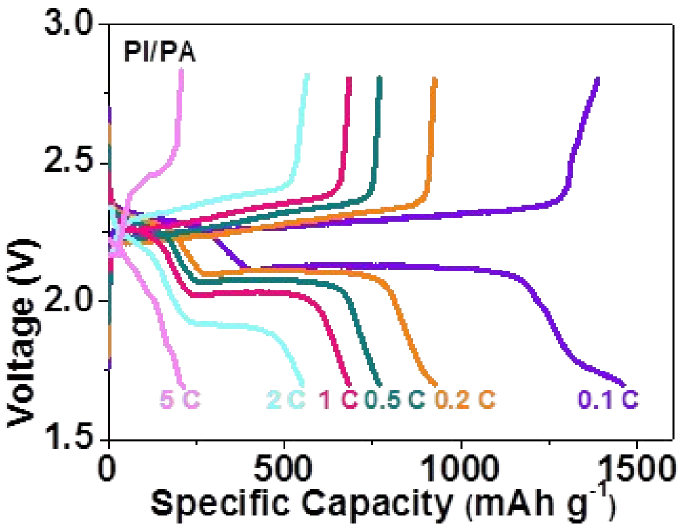

Figure S10. Discharge-charge profiles of Li-S batteries with the PI/PA separator at different rates.

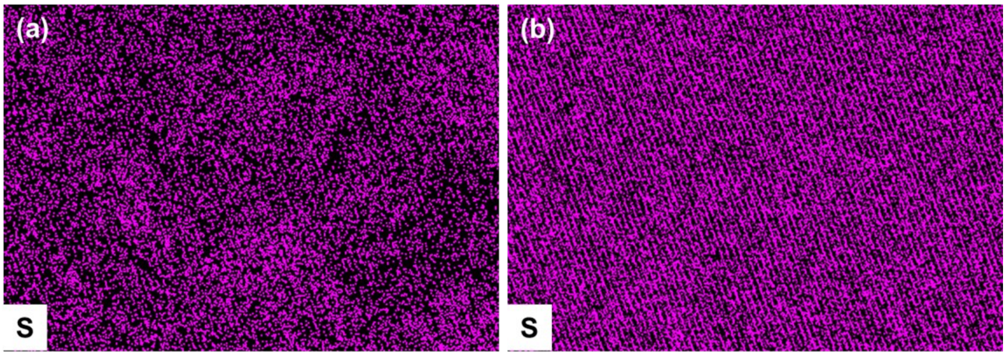

Figure S11. Elemental mappings of sulfur on the cathode faced with (a) Celgard and (b) PI/PA-PVA separators after rate test.

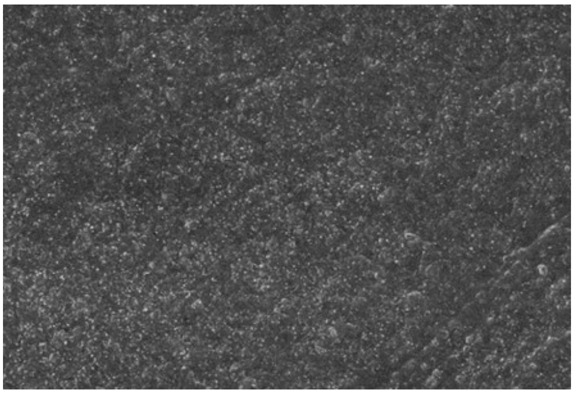

Figure S12. SEM image of the pristine lithium anode.

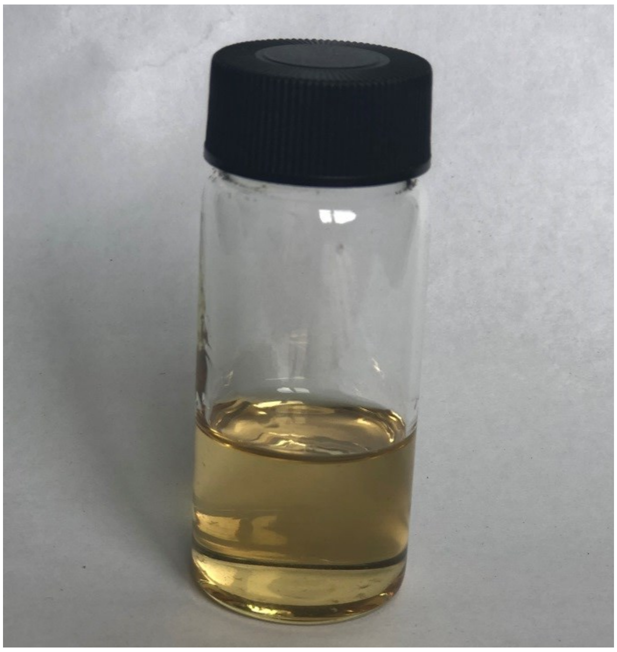

Figure S13. Photograph of the synthesized PAA in NMP solution (15%).

Table S1. Physical properties of different separators.

Membrane	Thickness (μm)	Porosity (%)	Contact angle (º)	Electrolyte uptake (%)	Electrolyte retention (%)
PI	30 ± 0.5	92.1 ± 0.5	0	2011	70.2
PI/PA	30 ± 0.5	76.6 ±0.5	35.8	1321	41.1
PI/PA-PVA	30 ± 0.5	75.1 ± 0.5	0	1640	52.6
Celgard	25 ± 0.5	41.3 ± 0.5	49.2	156	11.5

Table S2. Electrochemical performance comparison of this work with the previous reports involving different separators using carbon-sulfur cathodes in Li-S batteries.

Separator	**Sulfur (%)**	**Initial capacity [mA h g^{-1}] (Current rate)**	**Rate capability [mA h g^{-1}] (Cycling rate)**	**Fading rate per cycle (%)**	**Refs**
CNT/PP [a]	60	1179(0.1 C)	430 (2 C)	0.4 (100 cycles, 0.1C)	1
Black phosphorus/Celgard	80	930 (0.4 A g^{-1})	623(3.5 A g^{-1})	0.14 (100 cycles, 0.1 C)	2
AC/GF [b]	70	1324 (0.2 C)	362 (1.5 C)	0.8 (50 cycles, 0.2 C)	3
PAA-SWNT/Celgard [c]	65	1130(0.1 C)	592 (2 C)	0.13 (100 cycles, 0.2 C)	4
TiN/Celgard	60	1061 (0.5 C)	329 (2 C)	0.15 (250 cycles, 0.5 C)	5
MEC-AA [d]	70	915 (0.5 C)	720 (1 C)	0.2 (150 cycles, 0.5 C)	6
KB@Ir/Celgard [e]	75	1600 (0.1 C)	653 (2 C)	0.25 (100 cycles, 0.2C)	7
MoS_2/Celgard	65	1471 (0.1 C)	550(1 C)	0.08 (600 cycles, 0.5C)	8
SiO_2/PP	60	937 (0.2 C)	621 (1 C)	0.23 (200 cycles, 0.2 C)	9
PI/PA-PVA	**70**	**1499 (0.1 C)**	**497 (5 C)**	**0.1 (500** cycles**, 0.2 C)**	**This work**

[a] PP: Polypropylene

[b] AC/GF: Biomass-derived porous carbon / glass fiber

[c] PAA-SWNT/Celgard: Poly(acrylic acid) coated single-walled carbon nanotube film on Celgard.

[d] MEC-AA: MCM-41/ carbon nanotubes wrapped poly-(ether imide) nanofibers

[e] KB@Ir/Celgard: Ketchen Black and Ir nanoparticle modified Celgard

Table S3. Specific conditions of the interfacial polymerization for different samples.

Samples	Monomer concentration		
	TMC (mM)	PZ (mM)	PVA (mM)
PI	60	1179(0.1 C)	430 (2 C)
PI/PA	80	930 (0.4 A g^{-1})	623(3.5 A g^{-1})
PI/PA-PVA	70	1499 (0.1 C)	497 (5 C)

References

1. B. Liu, X. M. Wu, S. Wang, Z. Tang, Q. L. Yang, G. H. Hu and C. X. Xiong, *Nanomater.*, 2017, **7**, 196.
2. J. Sun, Y. M. Sun, M. Pasta, G. M. Zhou, Y. Z. Li, W. Liu, F. Xiong and Y. Cui, *Adv. Mater.*, 2016, **28**, 9797-9803.
3. R. K. Selvan, P. Zhu, C. Yan, J. D. Zhu, M. Dirican, A. Shanmugavani, Y. S. Lee and X. W. Zhang, *J. Colloid Interface Sci.*, 2018, **513**, 231-239.
4. J. H. Kim, J. Seo, J. Choi, D. Shin, M. Carter, Y. Jeon, C. W. Wang, L. B. Hu and U. Paik, *ACS Appl. Mater. Interfaces*, 2016, **8**, 20092-20099.
5. X. He, Y. Shuai, L. Na, K. H. Chen, Y. Q. Zhang, Z. P. Zhang and F. Y. Gan, *Mater. Lett.*, 2018, **215**, 91-94.
6. J. H. Kim, G. Y. Jung, Y. H. Lee, J. H. Kim, S. Y. Lee, S. K. Kwak and S. Y. Lee, *Nano Lett.*, 2017, **17**, 2220-2228.
7. P. J. Zuo, J. F. Hua, M. X. He, H. Zhang, Z. Y. Qian, Y. L. Ma, C. Y. Du, X. Q. Cheng, Y. Z. Gao and G. P. Yin, *J. Mater. Chem. A*, 2017, **5**, 10936-10945.
8. Z. A. Ghazi, X. He, A. M. Khattak, N. A. Khan, B. Liang, A. Iqbal, J. X. Wang, H. Sin, L. S. Li and Z. Y. Tang, *Adv. Mater.*, 2017, **29**, 1606817.
9. J. Li, Y. D. Huang, S. Zhang, W. Jia, X. C. Wang, Y. Guo, D. Z. Jia and L. S. Wang, *ACS Appl. Mater. Interfaces*, 2017, **9**, 7499-7504.